

# RSC Advances



This is an *Accepted Manuscript*, which has been through the Royal Society of Chemistry peer review process and has been accepted for publication.

*Accepted Manuscripts* are published online shortly after acceptance, before technical editing, formatting and proof reading. Using this free service, authors can make their results available to the community, in citable form, before we publish the edited article. This *Accepted Manuscript* will be replaced by the edited, formatted and paginated article as soon as this is available.

You can find more information about *Accepted Manuscripts* in the [Information for Authors](#).

Please note that technical editing may introduce minor changes to the text and/or graphics, which may alter content. The journal's standard [Terms & Conditions](#) and the [Ethical guidelines](#) still apply. In no event shall the Royal Society of Chemistry be held responsible for any errors or omissions in this *Accepted Manuscript* or any consequences arising from the use of any information it contains.

## Synthesis of nickel carbonate hydroxide/zeolitic imidazolate framework-8 as a supercapacitors electrode

Yilong Gao <sup>a</sup>, Jianxiang Wu <sup>a</sup>, Wei Zhang <sup>a</sup>, Yueyue Tan <sup>a</sup>, Jing Gao <sup>b</sup>, Bohejin Tang <sup>a,\*</sup>  
and Jiachang Zhao <sup>a</sup>

<sup>a</sup> College of Chemistry and Chemical Engineering, Shanghai University of Engineering Science, Shanghai 201620, China

<sup>b</sup> Analysis and Determination Center, Changsha Research Institute of Mining and Metallurgy limited liability company, Changsha 410012, China

\*Corresponding author : Tel: +86-021-67791214 Fax: +86-021-67791214

\*E-mail address: tangbohejin@sues.edu.cn

**The zeolitic imidazolate framework-8 (ZIF-8), nickel carbonate hydroxide ( $\text{Ni}_2\text{CO}_3(\text{OH})_2$ ) and  $\text{Ni}_2\text{CO}_3(\text{OH})_2/\text{ZIF-8}$  composite material are synthesized by a typical solvothermal method. In the  $\text{Ni}_2\text{CO}_3(\text{OH})_2/\text{ZIF-8}$  material, the ZIF-8 acts as the host for the growth of  $\text{Ni}_2\text{CO}_3(\text{OH})_2$ . Their structure and surface morphology are characterized by X-ray diffraction, scanning electron microscopy, transmission electron microscopy and nitrogen adsorption-desorption isotherms. The porous structure combined with  $\text{Ni}_2\text{CO}_3(\text{OH})_2$  maximizes the utilization of active material, resulting in a high specific capacitance. As electrode materials for supercapacitors, the ZIF-8,  $\text{Ni}_2\text{CO}_3(\text{OH})_2$  and  $\text{Ni}_2\text{CO}_3(\text{OH})_2/\text{ZIF-8}$  electrodes exhibit a specific capacitance of 140, 668 and 851  $\text{F g}^{-1}$  respectively at a scan rate of 5  $\text{m V s}^{-1}$  and good stability**

**over 5000 cycles. In particular, Ni<sub>2</sub>CO<sub>3</sub>(OH)<sub>2</sub>/ZIF-8 is a promising candidate for the supercapacitor electrode.**

The challenges of meeting the rapidly increasing demands for energy and developing carbon-neutral economy require untiring efforts to exploit renewable and clean energy storage devices <sup>1</sup>. Supercapacitors are considered as a promising candidate in the electrical energy storage field due to their high power density, long cycle life and safety tolerance to high rate charge and discharge <sup>2</sup>. Energy storage mechanisms of supercapacitors are divided into two ways, double-layer capacitance arising from the charge separation at an electrode/electrolyte interface and pseudocapacitance arising from fast, reversible faradaic reactions occurring at or near a solid electrode surface <sup>3</sup>. According to the energy storage mechanisms of double-layer capacitance and pseudocapacitance, the materials for supercapacitors should possess a high specific surface area to enhance the charge-storage capability.

Currently, metal-organic frameworks (MOFs) have gained particular attention in recent years as a novel class of nanoporous materials mainly because of their designable framework structures modularly built from transition-metal clusters as nodes and organic ligands as struts. As one of them, ZIF-8 has great properties such as large pore size (diameter of 11.6 Å), and large surface area (BET, 1413 m<sup>2</sup>/g), high thermal stability (up to 550 °C), and remarkable chemical resistance to boiling alkaline water and organic solvents <sup>4</sup>. The applications of ZIF-8 in gas separation <sup>5,6</sup>, catalysis <sup>7,8</sup>, and sensing <sup>9</sup> have been recently reported. However, there are a limited number of reports on MOFs as supercapacitor electrode Materials up to now <sup>10-12</sup>. In

recent years, Nickel hydroxyl compounds materials are typical active materials for electrochemical capacitors<sup>13-17</sup>, which generate specific capacitance (SC) on Faradaic pseudo mechanism. Most of them display excellent electrochemical performance. For example, mesoporous  $\alpha$ -Ni(OH)<sub>2</sub> has a maximum specific capacitance of 1718 F g<sup>-1</sup> at a scan rate of 5 mV s<sup>-1</sup><sup>18</sup>. Ni<sub>2</sub>CO<sub>3</sub>(OH)<sub>2</sub>, one of nickel hydroxyl compounds, is only as precursor to prepare nanostructured nickel compounds for supercapacitor electrode<sup>19-22</sup>. In the light of most metal hydroxides having large theoretical SC values<sup>17</sup>, we consider that Ni<sub>2</sub>CO<sub>3</sub>(OH)<sub>2</sub> has a potential as electrode materials for supercapacitor.

In our previous study<sup>23</sup>, ZIF-8 has been investigated as electrode materials for supercapacitor. Herein, Ni<sub>2</sub>CO<sub>3</sub>(OH)<sub>2</sub> and Ni<sub>2</sub>CO<sub>3</sub>(OH)<sub>2</sub>/ZIF-8 are synthesized via a typical solvothermal method and investigated as potential electrode materials for supercapacitors with KOH electrolyte, respectively. The Ni<sub>2</sub>CO<sub>3</sub>(OH)<sub>2</sub>/ZIF-8 composite material shows excellent electrochemical properties with specific capacitance of 851 F g<sup>-1</sup> at a scan rate of 5 mV s<sup>-1</sup> and excellent cycling performance.

The crystal structure and purity of the samples were examined by powder XRD analysis in Fig. 1. A sharp peak at  $\theta=7.2^\circ$  is observed on the XRD diffractogram of the ZIF-8, indicating that a highly crystalline material is achieved. The XRD pattern of the as synthesized ZIF-8 in this work is match up with the patterns from the single crystal data of pure ZIF-8<sup>4</sup>. The difference of peaks intensity is due to the crystal preferred orientation. And the XRD pattern shown in Fig. 1d suggests that the obtained product is nickel carbonate hydroxide [Ni<sub>2</sub>CO<sub>3</sub>(OH)<sub>2</sub>] (JCPDS 35-0501).

Fig. 1c is the XRD pattern of  $\text{Ni}_2\text{CO}_3(\text{OH})_2/\text{ZIF-8}$ , which shows that the  $\text{Ni}_2\text{CO}_3(\text{OH})_2$  successfully loaded onto ZIF-8. Though the pattern of  $\text{Ni}_2\text{CO}_3(\text{OH})_2/\text{ZIF-8}$  is a little different from the as synthesized ZIF-8, it is worth noting the crystalline order of the ZIF-8 host matrix mostly remains unchanged after loading  $\text{Ni}_2\text{CO}_3(\text{OH})_2$ , as shown by the comparison of the powder XRD patterns. No obvious diffractions are detected for  $\text{Ni}_2\text{CO}_3(\text{OH})_2$  species from powder XRD patterns in  $\text{Ni}_2\text{CO}_3(\text{OH})_2/\text{ZIF-8}$  samples, which may indicate  $\text{Ni}_2\text{CO}_3(\text{OH})_2$  loadings are dispersed uniformly or too little in the samples. The morphology of the  $\text{Ni}_2\text{CO}_3(\text{OH})_2$  and  $\text{Ni}_2\text{CO}_3(\text{OH})_2/\text{ZIF-8}$  were examined by SEM and TEM. As shown in Fig. 2, the cotton-like structure with fibers as primary structures, shows loosely packed microstructure morphology characteristics. Nitrogen adsorption-desorption isotherms are shown in Fig. 3. The BET surface area of  $\text{Ni}_2\text{CO}_3(\text{OH})_2$  and  $\text{Ni}_2\text{CO}_3(\text{OH})_2/\text{ZIF-8}$  are  $156.7 \text{ m}^2 \text{ g}^{-1}$  and  $313.8 \text{ m}^2 \text{ g}^{-1}$ , respectively.

Cyclic voltammetry (CV) is considered as an important method in supercapacitor to evaluate the potential possibility of materials used for capacitive deionization and helps to obtain the electrochemical properties such as specific capacitance. Fig. 4(a-c) shows the CV curves of the active materials electrode in 6 M KOH electrolyte at various scan rates from  $5 \text{ mV s}^{-1}$  to  $30 \text{ mV s}^{-1}$ . The CV shape of the electrode apparently reveals distinct pseudocapacitive characteristic, which is remarkably different from the closely ideal rectangular CV shape for an electric double-layer capacitor. Notably, a couple of redox peaks were observed within the potential range from 0 to 0.7 V, indicating that the electrochemical capacitance of the electrodes

mainly results from the pseudocapacitance. The reactions of ZIF-8 electrodes seem to proceed through the following mechanism<sup>24</sup> :



The  $\text{Ni}_2\text{CO}_3(\text{OH})_2$  electrode presents well-defined redox current peaks, and in line with the reversible reactions of  $\text{Ni}^{2+}/\text{Ni}^{3+}$ <sup>17, 25, 26</sup>. Clearly, with increasing scan rate, the anodic peaks of the electrodes shift positively, while their cathodic peaks shift negatively. However, solution and electrode resistance distort slightly the current response at the switching potential and this distortion is dependent upon the scan rate<sup>27</sup>, as can be seen from Fig. 4(b-c). The specific capacitances (SC) of electrodes are calculated according to the CV curves at different scan rates and the clear relationships are shown in Fig. 4(d). The SC value  $C$  can further be estimated according to the following equation<sup>28</sup> :

$$C = \frac{1}{vm} \int \frac{I}{V} dV \quad (2)$$

Where  $C$  is the specific capacitance ( $\text{F g}^{-1}$ ),  $v$  is the scan rate ( $\text{V s}^{-1}$ ),  $m$  is the mass of the active material (g),  $I$  and  $V$  are the current density (A) and the corresponding voltage (V), respectively. The SC values for the ZIF-8,  $\text{Ni}_2\text{CO}_3(\text{OH})_2$  and  $\text{Ni}_2\text{CO}_3(\text{OH})_2/\text{ZIF-8}$  electrodes are 140, 668 and  $851 \text{ F g}^{-1}$  at a scan rate of  $5 \text{ mV s}^{-1}$ , and decrease to 87, 322 and  $417 \text{ F g}^{-1}$  with increasing scan rate to  $30 \text{ mV s}^{-1}$ , respectively. For the ZIF-8, the spatial organization of metal ions and organic ligands leads to rationally designed frameworks with nanosized channels and cavities. This type of porous architecture is favorable for an easy to-and-fro diffusion of ions during charging/discharging process in a capacitor. Compared with pure ZIF-8 and

$\text{Ni}_2\text{CO}_3(\text{OH})_2$ , the  $\text{Ni}_2\text{CO}_3(\text{OH})_2/\text{ZIF-8}$  electrode shows much larger SC. This good pseudo-capacitive performance is mainly due to the synergistic electrochemical behavior of ZIF-8 and  $\text{Ni}_2\text{CO}_3(\text{OH})_2$ . ZIF-8 holds an intersecting three-dimensional structural feature, large surface area and large pore size. For these reasons the  $\text{Ni}_2\text{CO}_3(\text{OH})_2$  is well dispersed. Typically, the porous structure is favorable for fast ion/electron transfer. In addition, the cotton-like shape of the aggregate structure plays a basic role in the morphology requirement for electrochemical accessibility of electrolyte  $\text{OH}^-$  to  $\text{Ni}_2\text{CO}_3(\text{OH})_2$  active material and a fast diffusion rate within the redox phase. It is believed that the unique structure provides an important morphological foundation for the high SC.

Chronopotentiometry (CP) curves for the ZIF-8,  $\text{Ni}_2\text{CO}_3(\text{OH})_2$  and the  $\text{Ni}_2\text{CO}_3(\text{OH})_2/\text{ZIF-8}$  electrodes are shown in Fig. 5(a-c) at a current density of  $5 \text{ mA}\cdot\text{cm}^{-2}$ , respectively. The discharge curves of samples are not linear, suggesting the pseudocapacitive behavior of this electrode material, which is in agreement with CV analyses. The columbic efficiency is nearly 100% for each cycle of charge and discharge as can be seen from Fig. 5(a-c).

For further investigation of the actual electrochemical diffusion process, EIS spectra of the ZIF-8,  $\text{Ni}_2\text{CO}_3(\text{OH})_2$  and the  $\text{Ni}_2\text{CO}_3(\text{OH})_2/\text{ZIF-8}$  electrodes are measured in the frequency range from 0.01 to  $10^5$  Hz at open circuit potential with an ac excitation signal of 5 mV, as shown in Fig.5(d). A single semicircle in the high frequency region is due to the internal resistance and capacitance. A linear inclination in the low frequency region is due to diffusion of electrolyte ions. The solution

resistance  $R_s$  and the charge transfer resistance  $R_{ct}$  can be obtained from the Nyquist plot, where the high frequency semicircle intercepts the real axis at  $R_s$  and  $(R_s+R_{ct})$ , respectively. As shown in Fig. 5(d), the  $R_s$  are almost same, namely, 0.5  $\Omega$ , for  $Ni_2CO_3(OH)_2$  and the  $Ni_2CO_3(OH)_2/ZIF-8$  electrodes, and the  $R_s$  of the ZIF-8 electrode is 0.6  $\Omega$ . More importantly, the  $R_{ct}$  of  $Ni_2CO_3(OH)_2/ZIF-8$  electrode is less than the  $Ni_2CO_3(OH)_2$  electrode's.

The specific capacitance as a function of cycle number is plotted in Fig. 6. It is observed that the specific capacitance of the ZIF-8 electrode continuously increases until about 700<sup>th</sup> cycle. The capacitance of  $Ni_2CO_3(OH)_2$  and  $Ni_2CO_3(OH)_2/ZIF-8$  electrode drop in this case are sharp at the beginning of 300 cycles and keeps slowly increasing till 2000 cycles, and then all the electrodes keep almost constant with slight fluctuations up to 5000 cycles. The capacitance decrease in the initial stage is possibly due to certain irreversible reaction in electrochemical process and increase in the following cycles is a full-activation at the electrode/electrolyte interface. The results show that the specific capacitances obtained from  $Ni_2CO_3(OH)_2/ZIF-8$  sample is superior to those derived from synthesized pure ZIF-8 and  $Ni_2CO_3(OH)_2$  materials.

## Conclusion

In summary, we have demonstrated  $Ni_2CO_3(OH)_2/ZIF-8$  was successfully synthesized via a solvothermal method and as a supercapacitor electrode for the first time, respectively. XRD, SEM, TEM, Nitrogen adsorption-desorption isotherms and Electrochemical tests were employed to characterize the composite materials. The

results show that the introduction of the ZIF-8 into  $\text{Ni}_2\text{CO}_3(\text{OH})_2$  could enhance both specific capacitance and electrochemical stability of the  $\text{Ni}_2\text{CO}_3(\text{OH})_2/\text{ZIF-8}$  composite electrodes. We expect that it bring light to new opportunities in the development of high performance energy storage devices by using rapidly growing MOFs as supports. Work is underway to expand ZIF-8 to other host MOFs for electrochemistry.

### Experimental section

Synthesis method of ZIF-8 ( $\text{Zn}(\text{N}_2\text{C}_4\text{H}_6)_2$ ) was according to the literature of Yaghi et al <sup>4</sup>. The process of  $\text{Ni}_2\text{CO}_3(\text{OH})_2/\text{ZIF-8}$  complexes were the following: synthesized by mixing ZIF-8 and  $\text{Ni}(\text{NO}_3)_2 \cdot 6\text{H}_2\text{O}$  (mass ratio=1:2) with 10 ml deionized water and the resulting mixtures were stirred at 293 K for about 2 h. Then,  $\text{Na}_2\text{CO}_3$  solutions (0.3 mol/L) were feeded into Teflon-lined and the molar ratio of  $\text{Ni}^{2+}/\text{CO}_3^{2-}$  can varied from 1:1.1 to 1:1.3. When the addition was completed, the mixed solution adjusted to pH=8.0-8.5 with ammonium hydroxide. The slurry was aged in dilute ammonia at 373 K in autoclave for at least 10 h. After being aged, the slurry was filtrated and dried. Then the dried precipitate was rewashed by hot water several times till the filtrate was almost clear when being detected by silver nitrate solution, and redried at 398 K in air flow. At last the dried green precipitate was grinded to get the finished product. As a control,  $\text{Ni}_2\text{CO}_3(\text{OH})_2$  was also synthesized by the same method as described above, except that there was no ZIF-8 involved.

The working electrode was prepared by mixing 75 wt.% of the synthesized

active material powder, 20 wt.% of acetylene black and 5 wt.% of poly(tetrafluoroethylene). After that, the resulting paste was immersed into a nickel foam (1 cm<sup>2</sup>) served as a current collector under a pressure of 10 MPa. The prepared electrode was dried at 90°C oven for 2 h. The electrode of ZIF-8, Ni<sub>2</sub>CO<sub>3</sub>(OH)<sub>2</sub> and Ni<sub>2</sub>CO<sub>3</sub>(OH)<sub>2</sub>/ZIF-8 contained about 3.75, 5.925 and 4.65 mg electroactive materials respectively and had a geometric surface area of 1 cm<sup>2</sup>.

Powder XRD data were collected on a Deutschland BRUKER D2 PHASER X-Ray Diffractometer with Cu K $\alpha$  radiation. The 2 $\theta$  was scanned in the range of 5-80° with a resolution of 0.02°s<sup>-1</sup>. Scanning electron microscopy (SEM) analysis (FEI INSPECT S50) was used to capture and determine the morphologies of the samples. The transmission electron microscopy (TEM) images were obtained on a Hitachi H-800 transmission electron microscope at an acceleration voltage of 200 kV. Nitrogen adsorption–desorption measurements for the products were performed using a Micromeritics ASAP 2460 instrument with a degassing temperature of 473 K, and using Barrett–Emmett–Teller (BET) calculations for the surface area. The pseudocapactive properties of the electrode were studied using cyclic voltammogram (CV), galvanostatic charge/discharge test and electrochemical impedance spectroscopy (EIS) in 6 M KOH aqueous solution. CVs and galvanostatic charge/discharge tests were conducted using the CHI660D electrochemical analyzer using a three-electrode configuration with the active material powder electrode as working electrode, platinum sheet as counter electrode and Ag as reference electrode<sup>12</sup>. The EIS measurements were conducted for the working electrode in a frequency

range of 100 kHz to 0.01 Hz with ac perturbation of 5 mV.

### Acknowledge

This work was supported by the Fund of Graduate Innovation Project, College of Chemistry and Chemical Engineering, Shanghai University of Engineering Science (A-0903-13-01078).

### References

1. N. S. Lewis and D. G. Nocera, *Proceedings of the National Academy of Sciences*, 2006, **103**, 15729-15735.
2. P. Simon and Y. Gogotsi, *Nat. Mater.*, 2008, **7**, 845-854.
3. B. E. Conway, *J. Electrochem. Soc.*, 1991, **138**, 1539-1548.
4. K. S. Park, Z. Ni, A. P. Cote, J. Y. Choi, R. Huang, F. J. Uribe-Romo, H. K. Chae, M. O'Keeffe and O. M. Yaghi, *Proc. Natl. Acad. Sci. U. S. A.*, 2006, **103**, 10186-10191.
5. H. Bux, F. Liang, Y. Li, J. Cravillon, M. Wiebcke and J. r. Caro, *J. Am. Chem. Soc.*, 2009, **131**, 16000-16001.
6. S. R. Venna and M. A. Carreon, *J. Am. Chem. Soc.*, 2009, **132**, 76-78.
7. H.-L. Jiang, B. Liu, T. Akita, M. Haruta, H. Sakurai and Q. Xu, *J. Am. Chem. Soc.*, 2009, **131**, 11302-11303.
8. C. Chizallet, S. Lazare, D. Bazer-Bachi, F. Bonnier, V. Lecocq, E. Soyer, A.-A. Quoineaud and N. Bats, *J. Am. Chem. Soc.*, 2010, **132**, 12365-12377.
9. G. Lu and J. T. Hupp, *J. Am. Chem. Soc.*, 2010, **132**, 7832-7833.
10. D. Y. Lee, S. J. Yoon, N. K. Shrestha, S.-H. Lee, H. Ahn and S.-H. Han,

- Microporous Mesoporous Mater.*, 2012, **153**, 163-165.
11. D. Y. Lee, D. V. Shinde, E.-K. Kim, W. Lee, I.-W. Oh, N. K. Shrestha, J. K. Lee and S.-H. Han, *Microporous Mesoporous Mater.*, 2013, **171**, 53-57.
  12. R. Díaz, M. G. Orcajo, J. A. Botas, G. Calleja and J. Palma, *Mater. Lett.*, 2012, **68**, 126-128.
  13. C.-C. Hu, J.-C. Chen and K.-H. Chang, *J. Power Sources*, 2013, **221**, 128-133.
  14. D.-L. Fang, Z.-D. Chen, X. Liu, Z.-F. Wu and C.-H. Zheng, *Electrochim. Acta*, 2012, **81**, 321-329.
  15. L. Cao, L.-B. Kong, Y.-Y. Liang and H.-L. Li, *Chem. Commun.*, 2004, 1646-1647.
  16. S. Yang, X. Wu, C. Chen, H. Dong, W. Hu and X. Wang, *Chem. Commun.*, 2012, **48**, 2773-2775.
  17. L.-B. Kong, L. Deng, X.-M. Li, M.-C. Liu, Y.-C. Luo and L. Kang, *Mater. Res. Bull.*, 2012, **47**, 1641-1647.
  18. S. Xing, Q. Wang, Z. Ma, Y. Wu and Y. Gao, *Mater. Lett.*, 2012, **78**, 99-101.
  19. Y. Gu, Z. Lu, Z. Chang, J. Liu, X. Lei, Y. Li and X. Sun, *Journal of Materials Chemistry A*, 2013, **1**, 10655-10661.
  20. G. Zhang, L. Yu, H. E. Hoster and X. W. Lou, *Nanoscale*, 2013, **5**, 877-881.
  21. J. Zhu, J. Jiang, Y. Feng, G. Meng, H. Ding and X. Huang, *ACS Appl. Mater. Interfaces*, 2013, **5**, 2634-2640.
  22. J. Zhu, J. Jiang, J. Liu, R. Ding, H. Ding, Y. Feng, G. Wei and X. Huang, *J. Solid State Chem.*, 2011, **184**, 578-583.

23. Y. Gao, J. Wu, W. Zhang, Y. Tan, J. Zhao and B. Tang, *Mater. Lett.*, 2014, **128**, 208-211.
24. S. Horike, D. Umeyama and S. Kitagawa, *Acc. Chem. Res.*, 2013, **46**, 2376-2384.
25. U. M. Patil, K. V. Gurav, V. J. Fulari, C. D. Lokhande and O. S. Joo, *J. Power Sources*, 2009, **188**, 338-342.
26. J. Liu, C. Cheng, W. Zhou, H. Li and H. J. Fan, *Chem. Commun.*, 2011, **47**, 3436-3438.
27. M. Aghazadeh, A. N. Golikand and M. Ghaemi, *Int. J. Hydrogen Energy*, 2011, **36**, 8674-8679.
28. N. A. M. Barakat, A. G. El-Deen, G. Shin, M. Park and H. Y. Kim, *Mater. Lett.*, 2013, **99**, 168-171.

## Figure Captions

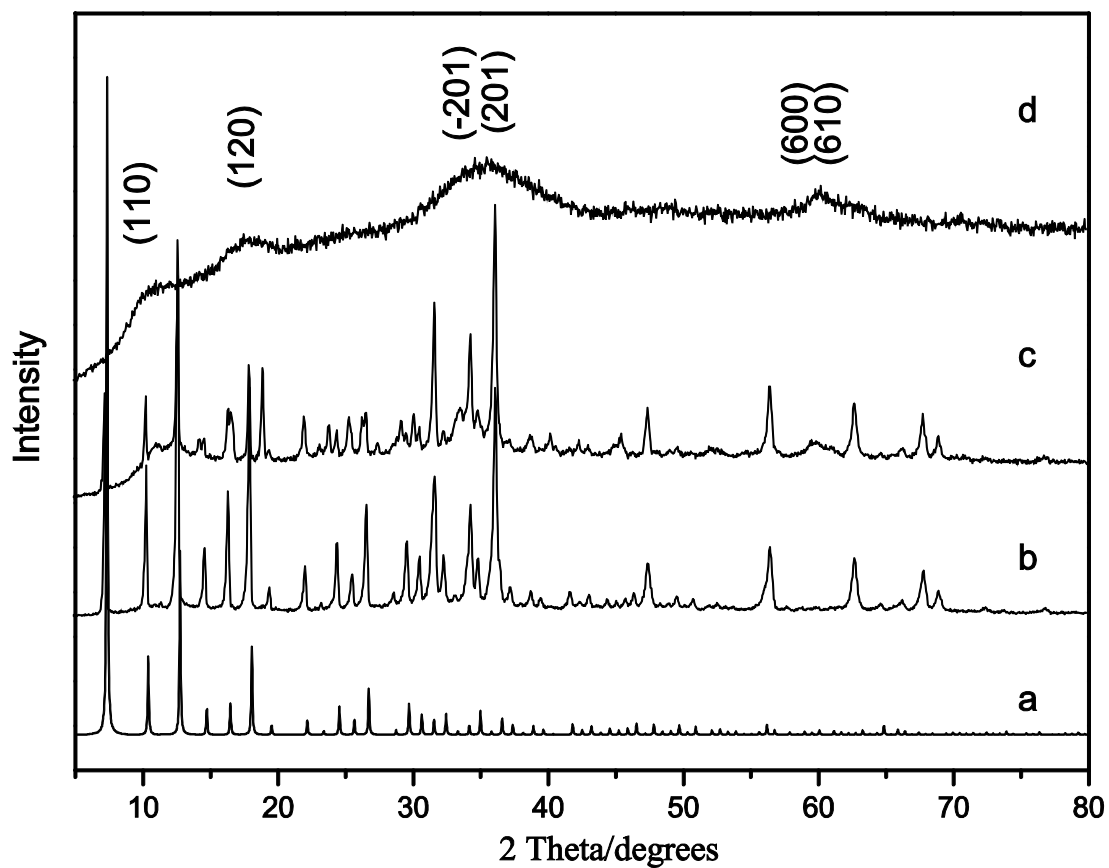


**Figure 1.** XRD patterns of (a) simulated ZIF-8; (b) as synthesized ZIF-8; (c)  $\text{Ni}_2\text{CO}_3(\text{OH})_2/\text{ZIF-8}$ ; (d)  $\text{Ni}_2\text{CO}_3(\text{OH})_2$ .

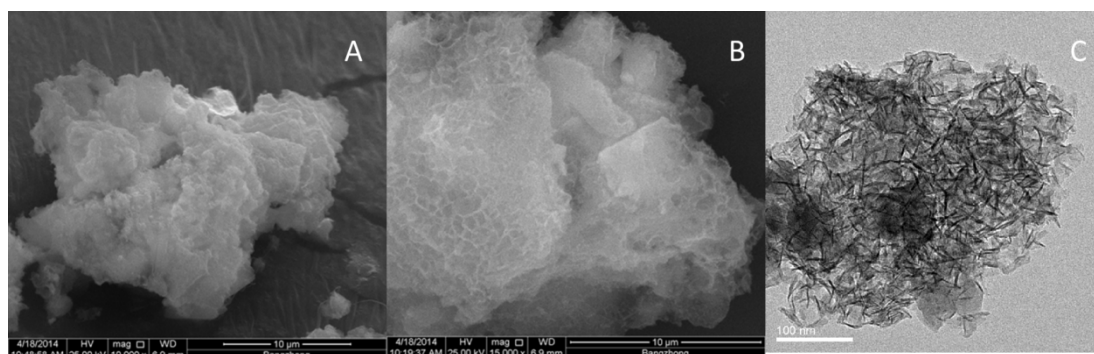


**Figure 2.** SEM images of (A)  $\text{Ni}_2\text{CO}_3(\text{OH})_2$ ; (B)  $\text{Ni}_2\text{CO}_3(\text{OH})_2/\text{ZIF-8}$ ; (C) TEM

images of  $\text{Ni}_2\text{CO}_3(\text{OH})_2/\text{ZIF-8}$ .

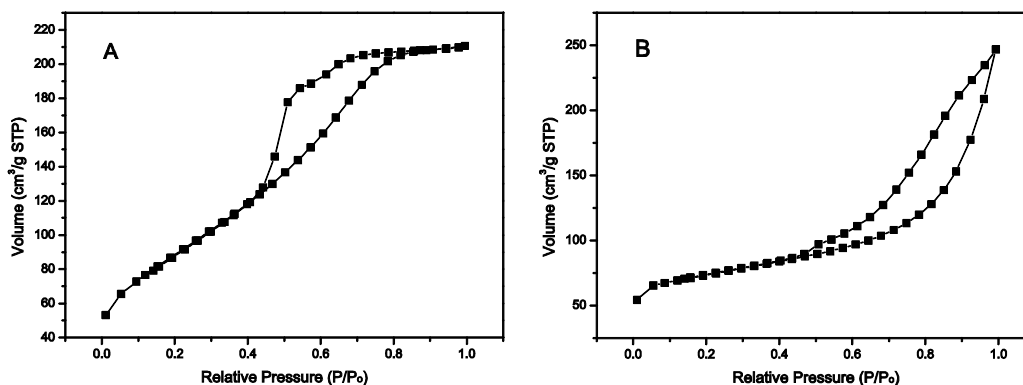


**Figure 3.** Nitrogen adsorption–desorption isotherm of (A)  $\text{Ni}_2\text{CO}_3(\text{OH})_2$ ; (B)  $\text{Ni}_2\text{CO}_3(\text{OH})_2/\text{ZIF-8}$ .

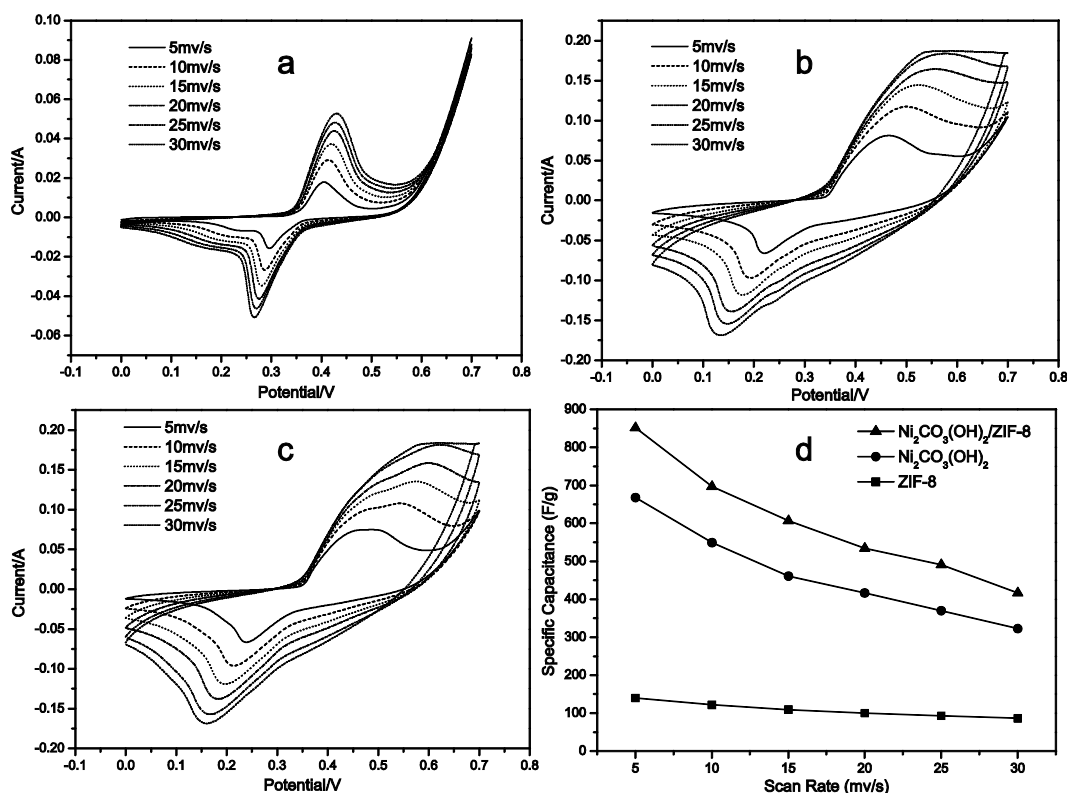


**Figure 4.** CV curves of different samples at various scanning rates. (a) experimental ZIF-8; (b)  $\text{Ni}_2\text{CO}_3(\text{OH})_2$ ; (c)  $\text{Ni}_2\text{CO}_3(\text{OH})_2/\text{ZIF-8}$ ; (d) The specific capacitance as a

function of scan rate of different samples.

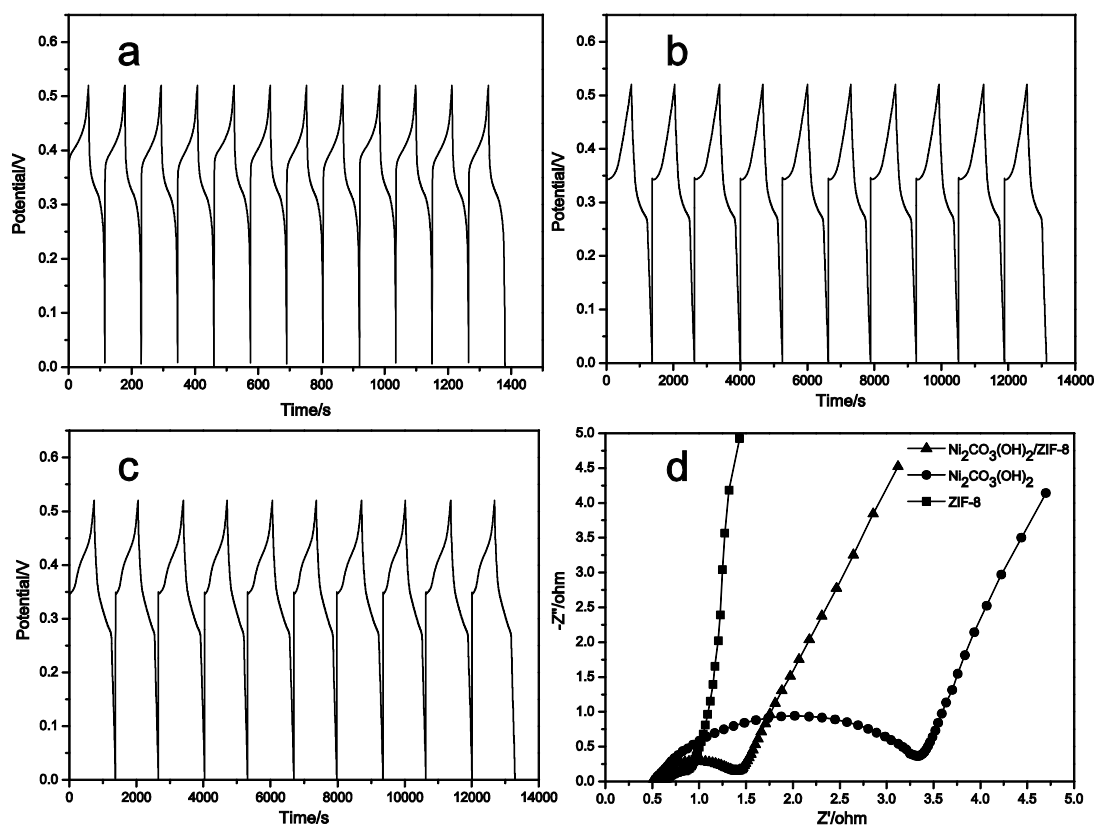


**Figure 5.** CP curves of (a) experimental ZIF-8; (b) Ni<sub>2</sub>CO<sub>3</sub>(OH)<sub>2</sub>; (c) Ni<sub>2</sub>CO<sub>3</sub>(OH)<sub>2</sub>/ZIF-8 at a current density of 5 mA·cm<sup>-2</sup>. (d) EIS spectra of the experimental ZIF-8, Ni<sub>2</sub>CO<sub>3</sub>(OH)<sub>2</sub>, Ni<sub>2</sub>CO<sub>3</sub>(OH)<sub>2</sub>/ZIF-8 electrodes.

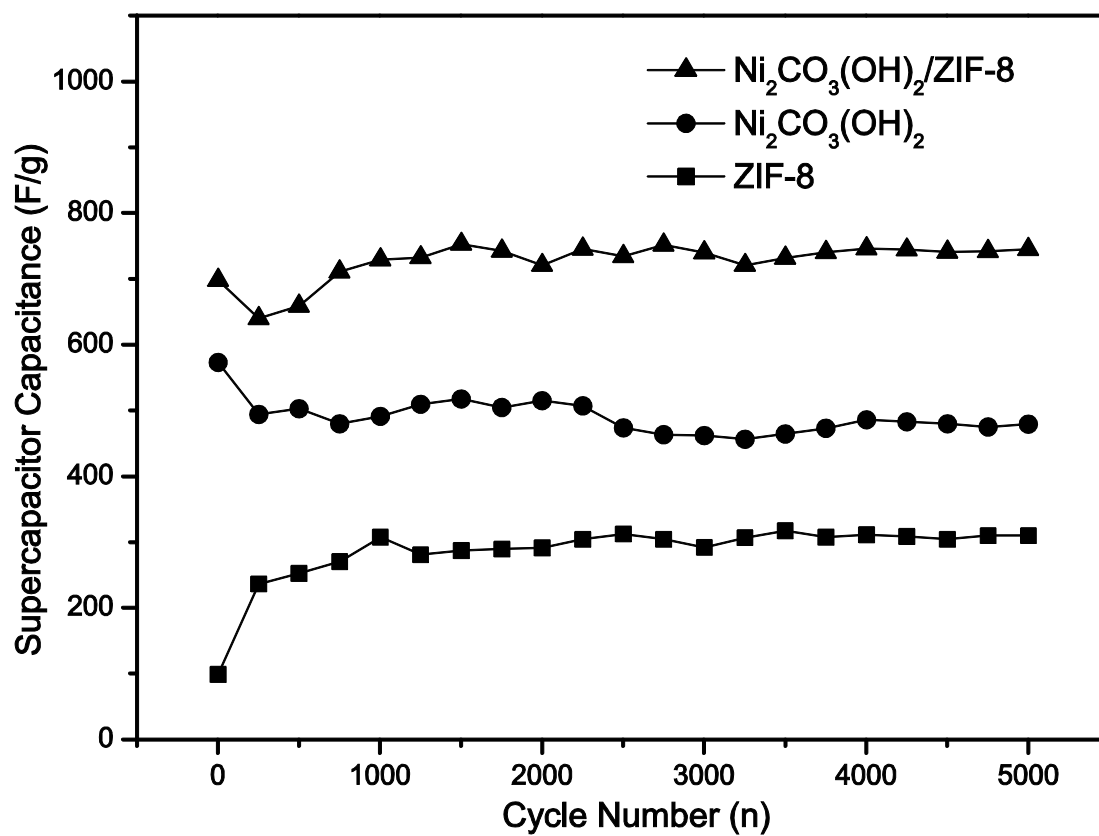


**Figure 6.** Cycling performance of samples at scan rate of  $10 \text{ mV s}^{-1}$ .